Available online at www.sciencedirect.com
ScienceDirect
Journal of Magnetic Resonance 188 (2007) 183–189
JMR Journal of Magnetic Resonance
www.elsevier.com/locate/jmr

Communication

Design and construction of a contactless mobile RF coil for double resonance variable angle spinning NMR

Chunqi Qian [a], Alex Pines [a], Rachel W. Martin [b,*]

[a] *Materials Science Division, Lawrence Berkeley National Laboratory, and Department of Chemistry, University of California, Berkeley, CA 94720, USA*
[b] *Department of Chemistry, University of California, Irvine, CA 92697-2025, USA*

Received 2 March 2007; revised 11 June 2007
Available online 30 June 2007

Abstract

Variable angle spinning (VAS) experiments can be used to measure long-range dipolar couplings and provide structural information about molecules in oriented media. We present a probe design for this type of experiment using a contactless resonator. In this circuit, RF power is transmitted wirelessly via coaxial capacitive coupling where the coupling efficiency is improved by replacing the ordinary sample coil with a double frequency resonator. Our probe constructed out of this design principle has shown favorable properties at variable angle conditions. Moreover, a switched angle spinning correlation experiment is performed to demonstrate the probe's capability to resolve dipolar couplings in strongly aligned molecules.

Keywords: Liquid crystal NMR spectroscopy; Variable angle spinning; NMR probe; Resonator; Capacitive coupling

1. Introduction

Variable angle spinning (VAS) experiments establish a correlation between isotropic and anisotropic spectra using off- and on-magic angle spinning. This technique was first introduced 25 years ago to extrapolate the quadrupolar couplings in solids from spectra obtained at different spinning angles [1]. A related method, switched angle spinning (SAS), was later adopted to measure the chemical shift anisotropy [2] and heteronuclear dipolar couplings [3] in solids by rapidly switching the sample spinning axis within the same experiment. It was later demonstrated that high-resolution spectra of quadrupolar nuclei could be measured by changing the spinning axis between two particular angles [4]. This is the principle of dynamic angle spinning [5], which is a special case of switched angle spinning. Recently, VAS methods have proven particularly useful in liquid crystals where the stochastic molecular motion makes rotor synchronized recoupling more difficult to achieve. It has been demonstrated that the director of a liquid crystal may be manipulated by changing the sample spinning axis [6], and that the anisotropic interactions are scaled by $(3\cos^2\theta-1)/2$, where θ is the angle between spinning axis and external magnetic field. The ability to change the molecular alignment tensor by variable angle spinning could allow scaling of dipolar coupling in strongly aligned molecules [7].

Although variable angle spinning is conceptually simple, its actual implementation presents several technical challenges. There are several requirements of an ideal variable angle probe. Firstly, we need a small sample coil that can reorient with the sample spinning axis in order to maximize the filling factor, instead of a big stationary coil as was used in the original design [8]. Secondly, a transverse coil is preferred over a standard solenoid so that constant B_1 field can be generated irrespective of the sample orientation [9]. Most importantly, we need a reliable RF junction to connect the mobile sample coil and the stationary tuning circuits. There have been continuous efforts to resolve this issue over the past 20 years, including sliding contact [10] and flexible power leads [11]. Both of these methods are

* Corresponding author. Fax: +1 949 824 9920.
E-mail address: rwmartin@uci.edu (R.W. Martin).

1090-7807/$ - see front matter © 2007 Elsevier Inc. All rights reserved.
doi:10.1016/j.jmr.2007.06.006

successful to a great extent, but over long-term use the sliding contact could suffer from the problem of arcing and oxidization at the contact surface, while the flexible leads would eventually introduce mechanical aging after many hops. As an alternative approach, we would like to introduce a design where the radio frequency is transmitted wirelessly via coaxial capacitive couplings. The core component of this design is a double frequency resonator which is coupled to stationary power transfer line via coaxial capacitors. The entire resonator containing the sample coil can reorient along an axis perpendicular to the external magnetic field. Here, we use a double frequency resonator, both because double resonance experiments are required, and because the resonator design improves the power transfer efficiency across the coupling capacitors. Since a transverse sample coil is used, the effective B_1 field remains constant regardless of the orientation angle of the coil.

In this communication, we first illustrate the design principle of our variable angle probe. We will then summarize its RF performance and analyze the major factors that affect the probe sensitivity. The double resonance capability is demonstrated by a solution state HSQC experiment with magic angle spinning. Finally, we report an example of dipolar local field spectroscopy with switched angle spinning methodology on a model system in a strongly oriented medium. The potential applications of our probe and improvements for future designs are also discussed.

2. Design principles

The simplest model for a single channel NMR probe is a lossless, impedance matched LC resonant circuit. In the presence of non-ideal components, the power dissipation on the series matching capacitor C_m is the major loss mechanism. If the single matching capacitor C_m is replaced by two series capacitors, each with a capacitance of $2C_m$, a balanced circuit can be obtained with the same resonance frequency. Balancing the circuit helps to even out the RF field profile along the length of the resonator [12], and also allows efficient power transfer on both sides of the coil even if it is not mechanically attached to the external circuit. This efficiency is optimized if the tuning capacitor C_t is on resonance with the coil L_s and if the quality factors of the coupling capacitors $2C_m$ are reasonably high.

The core of the double resonance circuit is two-frequency contactless resonator. One implementation of this resonator is shown in Fig. 1a. In this circuit, an additional series branch L_2–C_2 is introduced that has a resonance frequency slightly higher than the desired low frequency (LF). At high frequency, $\omega L_2 - 1/\omega C_2 > 0$ and the equivalent circuit is represented in Fig. 1b, where $\omega L_2' = \omega L_2 - 1/\omega C_2$. The power dissipation on the resonator is maximized at its high frequency self-resonance:

$$\omega_{HF} = \frac{1}{\sqrt{L_s C_t (\frac{L_2'}{L_s + L_2'})}}. \quad (1)$$

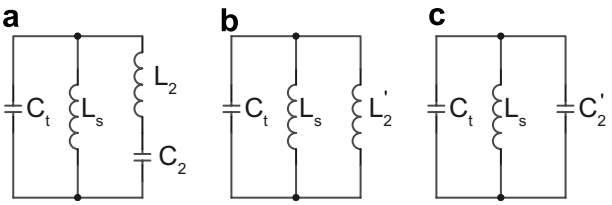

Fig. 1. (a) Schematic representation of double frequency contactless resonator. (b) Equivalent circuit of the resonator at high frequency (HF) where L_2' is the equivalent inductance. (c) Equivalent circuit of the resonator at low frequency (LF) where C_2' is the equivalent capacitance.

At low frequency, however, $\omega L_2 - 1/\omega C_2 < 0$ and the equivalent circuit is represented in Fig. 1c, where $1/\omega C_2' = 1/\omega C_2 - \omega L_2$. Now the power dissipation on the resonator is maximized at its low frequency self-resonance, which is represented by

$$\omega_{LF} = \frac{1}{\sqrt{L_s (C_t + C_2')}}. \quad (2)$$

Fig. 2 shows the geometrical arrangement of this resonator. The double-tuned resonator has two pairs of coaxial rings connected to the cylindrical sample coil, so that the high frequency and low frequency RF are transmitted from the left and right sides, respectively. The solenoid (L_2) is soldered to the outer metal ring directly at one end, and connected to the inner metal ring via a chip capacitor at the other end. This arrangement allows the sample coil to reorient inside the probe while maintaining the same capacitive coupling with the rest of the circuit at any spinning angle.

Once the contactless resonator is tuned, the remaining challenge is to impedance match this basic circuit with the power input. The resonator is impedance matched to 50 Ω using a network of variable transmission line segments [13]. Fig. 3 shows the complete circuit model for the entire double resonance probe. In order to ensure maximum isolation and minimum loss in sensitivity, the high frequency and low frequency inputs are placed at opposite ends of the sample coil. An open quarter wave tuned to the high frequency is used on the low-frequency side of the circuit in order to provide a ground path for the high frequency. If desired, a similar element tuned to the low frequency may be used on the opposite side of the coil. In principle, it is straightforward to extend the current design to multiple resonant circuits by combining a multiple frequency resonator and multiple frequency matching networks.

3. Results and discussion

Numerical simulation of the probe was helpful in predicting the B_1 conversion efficiency of the resonator. Because most of the components used in the resonator are distributed elements, we use the finite element method (FEM) for calculation. The commercial package COMSOL32 was used to calculate the electromagnetic field dis-

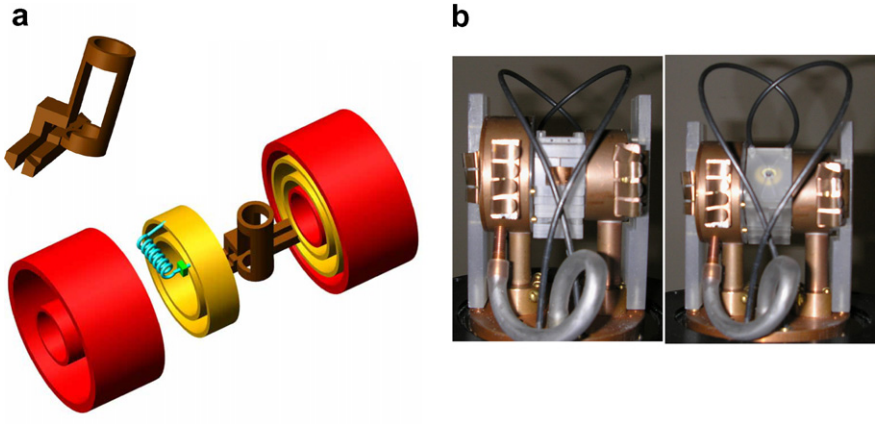

Fig. 2. (a) The physical layout of the capacitively coupled contactless resonator. The sample coil (brown) has a 4.7 mm inner diameter, 9.5 mm window height and 110° open angle. There are tuning capacitors on both sides of the coil. Each of the tuning capacitors is made of Teflon dielectrics sandwiched by coaxial copper rings (yellow). The OD of inner ring is 15.9 mm while the ID of the outer ring is 20.6 mm. Both rings are 6 mm long. The seven turn solenoid is made by wrapping a gauge 22 copper wire around a 1/16 inch diameter rod. The chip capacitor has a 39 pF capacitance. The resonator is capacitively coupled to the coaxial input (red) from the left and the right side. There is no mechanical contact between the yellow and red rings. (b) The stator assembly orienting at the zero degree and the magic angle. (For interpretation of the references to colour in this figure legend, the reader is referred to the web version of this article.)

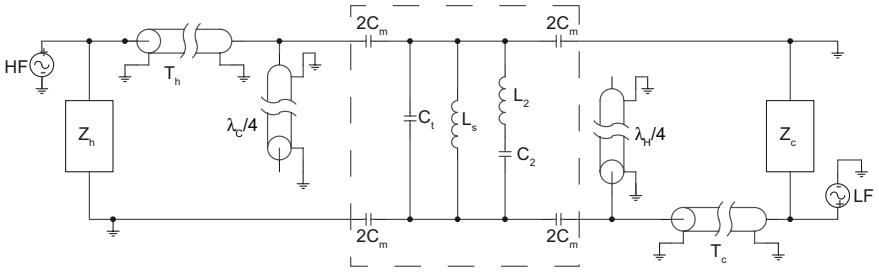

Fig. 3. The impedance matching network for double resonance probe. At high frequency, the contactless resonator (enclosed in dashed box) is impedance transformed by tunable transmission line T_h and matched to 50 Ω by shunt impedance Z_h. The same principle applies to the low frequency channel.

tribution with the input of the geometrical model and the proper choice of boundary conditions. In order to evaluate the coil efficiency, we define the figure of merit Ξ as the ratio between the square of B_1 field magnitude and the dissipated power through the input port. The ratio is indicative of the device's efficiency to transform its input power into the magnetic energy in the coil.

$$\Xi \equiv \frac{|B_1|^2}{\int_{\text{port}} (\vec{E} \times \vec{H}) \cdot \mathrm{d}\vec{S}} \tag{3}$$

Fig. 4 shows the simulation results for the frequency dependent behavior of Ξ at low and high frequencies. The precision of this type of calculation is strongly dependent on the level of details incorporated into the input model, which

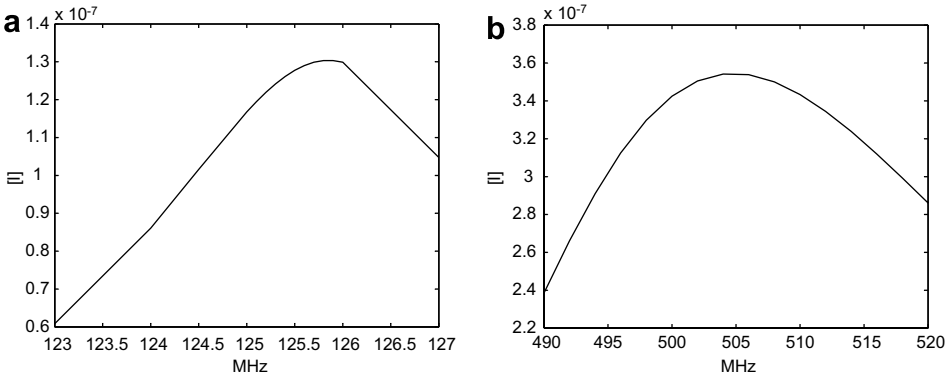

Fig. 4. Simulated frequency dependent behavior of figure of merit for the resonator geometry depicted in Fig. 2. (a) when low frequency input is used and (b) when high frequency input is used. FEM model is constructed and simulated by COMSOL32.

presents a challenge when simulating a circuit that has many stray reactances due to its complicated geometry. However, several useful qualitative results can be obtained. Firstly, the LF input channel has a maximum Ξ around 126 MHz and HF input channel has a maximum Ξ around 505 MHz. At 125.7 MHz, $\Xi \approx 1.3 \times 10^{-7}$ corresponds to a B_1 field of 3.6×10^{-3} T (39 KHz) with the input power of 100 W. At 500 MHz, $\Xi \approx 3.4 \times 10^{-7}$ corresponds to a B_1 field of 5.8×10^{-3} T (248 KHz) with the input power of 100 W. Therefore, in this resonator design, the HF nutation is 6.4 faster than the LF one. Secondly, if we define the optimum tuning range as the range within which Ξ is above 75% of its maximum, LF channel has a tuning range from 124.5 MHz to above 127 MHz (calculation for higher frequencies is not performed), while the HF channel has a tuning range from 492 MHz to above 520 MHz. As a prototype probe, we adopted a single turn Alderman-Grant coil because this type of resonator generates a low electric field at high frequencies [14]. This consideration is a high priority in investigations of semisolid biological samples because their high salt content leads to dielectric loss. Because of the high symmetry of this design, simulations are relatively straightforward. The resonator works better at higher frequencies because the coupling efficiency across coaxial capacitors is increased when the operating frequency goes up. At lower frequencies, this resonator has a much narrower tuning range that is slightly below the self-resonance frequency of serial branch L_2–C_2. In our 500 MHz probe, the tuning ranges at both frequencies are enough to ensure that we can tune the probe to ^{13}C and ^{1}H in samples with different electrical properties.

The experimental measurement demonstrates good tuning property. The input return loss of the proton channel is -35 dB, and the LF channel has a -30 dB return loss. The isolation between the channels is above -50 dB. The measured quality factor is 185 on HF channel and 118 on LF channel. In order to directly evaluate the B_1 homogeneity within the sample coil, a tiny droplet of water placed inside a sample holder was vertically moved along the coil cylindrical axis. Precise positioning of the water droplet is achieved by a position adjustment screw [15]. As is shown by Fig. 5a, 90% relative B_1 homogeneity could be achieved within the ± 3 mm region. This level of homogeneity is sufficient for a great many decoupling experiments that are sensitive to B_1 field deviations. The nutation curves in Figs. 5b and c again demonstrate the excellent homogeneity on both channels when the sample length is further restricted within a ± 1.7 mm region. In each case, the ratio of signals after effective 810° and 90° pulses is almost 100%. The two curves correspond to a 6 μs 90° time on proton channel and a 13.24 μs 90° time on carbon channel at power levels sufficient for experiments on samples in liquid crystalline media. When the probe is tested with the coil oriented at different angles, a constant B_1 field is generated and there is a maximum of 8% change in reflection voltage. This is in contrast to the conventional solenoid that has a vanishing efficiency when aligned along the external field.

In order to demonstrate the double resonance capability, we performed a ^{13}C, ^{1}H HSQC experiment on a 5 mM (U-^{13}C)-glucose in D_2O. The total sample volume is 8 μL and 200 Hz magic angle spinning is applied to remove the susceptibility broadening in sample of restricted length. Here, the slow spinning speed is chosen because the spinning is used only to remove magnetic susceptibility broadening. The spinning apparatus in this probe consists of a homebuilt stator using 4 mm rotors, as well drive and bearing hardware purchased from Varian Inc. (Fort Collins, CO). This hardware is capable of spinning at the fast MAS rates used for traditional solids experiments, however, we do not use this capability in these experiments. Our focus is on stable spinning at slower speeds, since we are using the spinning primarily to control the alignment of the director of liquid-crystalline samples, rather than to average out strong anisotropic interactions in solids.

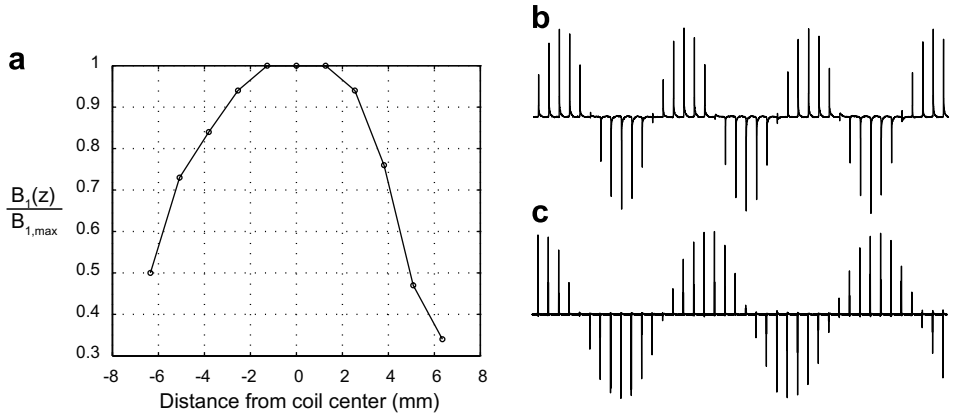

Fig. 5. (a) Measurement of B_1 homogeneity along z-axis of sample coil. The dots represent sampling points of 1.27 mm distance interval. When the sample length is restricted to 3.5 mm, the 810/90 ratio is nearly 100% on proton channel as demonstrated by the nutation curve in (b) and the 720/0 ratio is nearly 100% on the carbon channel as demonstrated by (c). The proton channel is calibrated with 8 μL of 2% H_2O/D_2O sample with the pulse length starts from 2 μs and increases at 2 μs per step. For the carbon channel, inverse calibration sequence was applied on a sample of 8 μL of 1 M (2-13C)-Gly. The carbon pulse width starts from 0.2 μs and increases by 3.26 μs for each step.

Because the experiment is performed in a wide bore solid state magnet, shimming was not performed to the standards of traditional solution state experiments. After 64 scans for each FID, a reasonably good 2D spectrum could be obtained (Fig. 6). Although our probe shows a modest sensitivity on a rather concentrated sample, our detection volume is only 1/40 of that of the conventional solution state probe and the line width here is ten times bigger than that could be obtained by a commercial probe with careful shimming. In our current application for dipolar local field experiments, the dipolar coupling is far bigger than the line width and the signal is strong enough for concentrated samples. Future probe designs will include susceptibility-compensated resonators with palladium-plated copper, as previously described [9,16]. In this way, the probe sensitivity could be greatly improved with enhanced resolution. Also, better manufacturing techniques combined with careful circuit optimization are crucial for further improvement of coil efficiency.

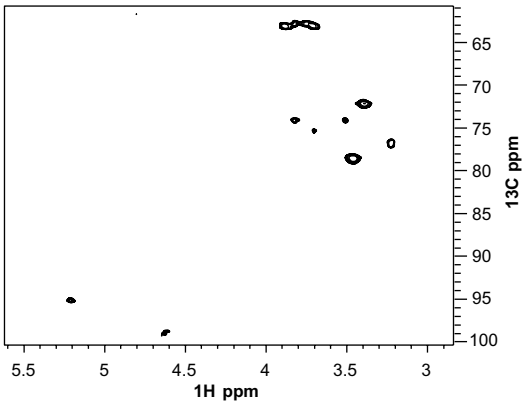

Fig. 6. ^{13}C,^{1}H HSQC experiment of a 5 mM solution of (U-^{13}C)-glucose in D_20, 298 K. Residual H_2O is suppressed by 50 Hz on resonance irradiation for 0.5 S before the sequence. Experimental parameters are $t_{1,\max} = 25.6$ ms, $t_{2,\max} = 102.4$ ms, relaxation delay between successive scans is 3 s. ^{13}C 90° time is 48 μs and ^{1}H 90° time is 11.8 μs. On the carbon channel, all inversion pulses are substituted by $90_x180_y90_x$ in order to achieve enhanced tolerance to off-resonance effect. The ^{13}C dimension spectrum width is 5 KHz and the carrier is set at 80 ppm so that the entire chemical shift range of glucose can be covered. ^{1}H dimension spectrum width is 5 KHz. WURST-40 decoupling is applied during signal acquisition. States-TPPI method is employed for frequency discrimination in the indirect dimension. ^{1}H frequency is 500.09 MHz, 64 scans per FID, Chemagnetics INFINITY spectrometer.

Because the experiment is performed in a wide bore solid state magnet, shimming was not performed to the standards of traditional solution state experiments. After 64 scans for each FID, a reasonably good 2D spectrum could be obtained (Fig. 6). Although our probe shows a modest sensitivity on a rather concentrated sample, our detection volume is only 1/40 of that of the conventional solution state probe and the line width here is ten times bigger than that could be obtained by a commercial probe with careful shimming. In our current application for dipolar local field experiments, the dipolar coupling is far bigger than the line width and the signal is strong enough for concentrated samples. Future probe designs will include susceptibility-compensated resonators with palladium-plated copper, as previously described [9,16]. In this way, the probe sensitivity could be greatly improved with enhanced resolution. Also, better manufacturing techniques combined with careful circuit optimization are crucial for further improvement of coil efficiency.

In order to demonstrate the switched angle capability of our probe, we performed a switched angle spinning experiment on acetonitrile dissolved in organic liquid crystal I52. We used a modified HETCOR sequence (Fig. 7) for our experiment. In this sequence, the rotor is first spinning at 0° during t_1 when the magnetization evolves on proton in the presence of frequency switched Lee Goldberg (FSLG) homonuclear decoupling. There is no inversion pulse on carbon channel during this time so that the heteronuclear dipolar coupling retains. In the optional delay after t_1, the magnetization is stored along the z-direction to allow sufficient dephasing of transverse magnetization and proton spin diffusion. The magnetization is then transferred to carbon by cross polarization and stored again as a longitudinal component before the second delay during which the rotor changes its spinning direction from the zero degree to the magic angle. SPINAL-64 [17] decoupling is

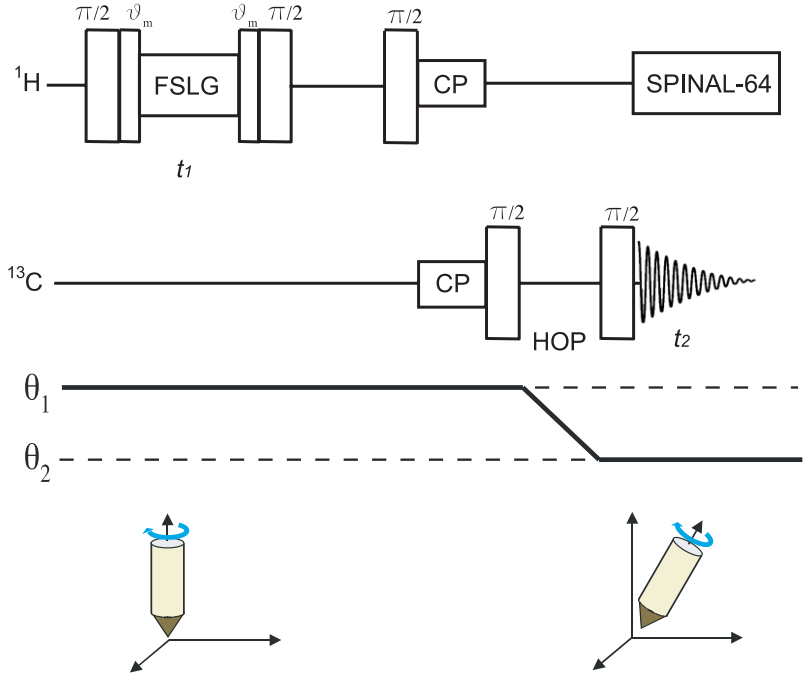

Fig. 7. Undecoupled HETCOR with switched angle spinning. The sample is spinning at 0° during t_1 period and spinning at magic angle during the detection period. The delay period for rotor hopping is 150 ms.

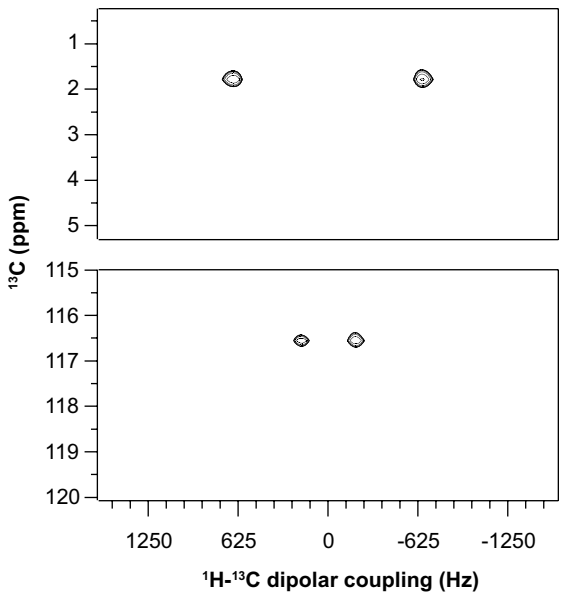

Fig. 8. Switched angle spinning HETCOR spectrum. The sample is a mixture of (1-^{13}C) CH_3CN and (2-^{13}C) CH_3CN dissolved in organic liquid crystal I52, with the concentration of each labeled species to be 6.8% (v/v). The total sample volume is 18 μL. For simplicity, the proton carrier frequency is set on resonance to the methyl chemical shift value. ^{13}C 90° time is 15.1 μs and ^{1}H 90° time is 11.8 μs. During t_1 period, a Lee Goldberg spin lock field of 50.81 kHz is applied to achieve homonuclear decoupling. The spectral width in the indirect dimension is 3.176 kHz, while the spectrum width in the direct dimension is 25 kHz. SPINAL-64 decoupling is applied at 21.2 kHz during signal detection. Other experimental parameters are $t_{1,\max} = 10.07$ ms, $t_{2,\max} = 20.48$ ms, relaxation delay between successive scans is 2 s and 8 scans are acquired for each FID, 64 FID acquired for the whole spectrum. TPPI method is employed for frequency discrimination in the indirect dimension. Because of the application of FSLG homonuclear decoupling sequence, the apparent splitting in the indirect dimension is scaled by $\sqrt{3}$ relative to the actual coupling value.

applied during the signal detection period to remove heteronuclear dipolar coupling. Due to the axial symmetry of the coaxial capacitors, a constant B_1 field is generated at different angles without having to retune the probe. A moderate spinning speed of 1600 Hz was chosen so that the liquid crystal could be aligned along the spinning axis without being disrupted by too big a centrifugal force. The angular orientation is controlled by a stepping motor within ±0.1 degree.

Fig. 8 is the spectrum obtained by the undecoupled HETCOR sequence. The indirect dimension contains information about heteronuclear dipolar coupling while the direct dimension corresponds to the isotropic chemical shift. Since the sample is switching between off- and on-magic angle spinning during the same experiment, the anisotropic and isotropic dimension are directly correlated. This kind of correlation will enable us to assign a specific coupling value to a particular spin pair. In the current spectrum, the apparent splitting in the indirect dimension is 1311.2 Hz for the C–H pair in methyl group and 378.2 Hz for the coupling between the methyl proton and the nitrile carbon. After correction with the scaling factor, the actual value of the heteronuclear couplings are 2271.1 and 655.1 Hz, respectively. In the direct dimension, the methyl carbon has chemical shift at 1.8 ppm and the nitrile carbon has chemical shift at 116.6 ppm. This correlates well with the standard values in literature.

4. Conclusions

The contactless resonator represents a way to provide a homogeneous RF field with constant amplitude independent of the spinning angle. These circuits can be modeled effectively using the finite element method as a guide to the design. They can be double-tuned and paired with variable transmission line impedance matching networks for double resonance experiments. Future work will include improvement of resolution by using a susceptibility-compensated coil, and variable angle spinning experiments on molecules in strongly oriented media are on the way.

Acknowledgments

This work was supported by the Director, Office of Science, Office of Basic Energy Sciences, Materials Sciences Division, US Department of Energy under contract no DEAC03-76SF00098 and by the School of Physical Sciences, UC Irvine. The authors would like to acknowledge Dr. Kathy Durkin for granting us access to the COMSOL32 licensed to the College of Chemistry at UC-Berkeley. Special thanks to Dr. Josef Granwehr, Dr. Christian Hilty, Dr. Louis Bouchard and Dr. Dimitris Sakellariou and Dr. Gregory Park for their helpful discussion and comments during the course of this work.

References

[1] S. Ganapathy, S. Schramm, E. Oldfield, Variable-angle sample-spinning high-resolution NMR of solids, J. Chem. Phys. 77 (1982) 4360–4365.
[2] A. Bax, N.M. Szeverenyi, G.E. Maciel, Chemical shift anisotropy in powdered solids studied by 2D FT NMR with flipping of the spinning axis, J. Magn. Reson. 55 (1983) 494–497.
[3] T. Terao, H. Miura, A. Saika, Dipolar SASS NMR spectroscopy: separation of heteronuclear dipolar powder patterns in rotating solids, J. Chem. Phys. 85 (1986) 3816–3826.
[4] B.F. Chmelka, K.T. Mueller, A. Pines, J. Stebbins, Y. Wu, J.W. Zwanziger, O-17 NMR in solids by dynamic-angle spinning and double rotation, Nature 339 (1989) 42–43.
[5] K.T. Mueller, B.Q. Sun, G.C. Chingas, J.W. Zwanziger, T. Terao, A. Pines, DAS of quadrupolar nuclei, J. Magn. Reson. 86 (1990) 470.
[6] J. Courtieu, D.W. Alderman, D.M. Grant, J.P. Bayles, Director dynamics and NMR applications of nematic liquid crystals spinning at various angles from the magnetic field, J. Chem. Phys 77 (1982) 723–730.
[7] G.H.J. Park, R.W. Martin, D. Sakellariou, A. Pines, A.G. Shahkhatuni, A.A. Shakhatuni, H.A. Panosyan, Variable angle spinning (VAS) NMR study of solvent effects in liquid crystalline solutions of ^{13}C-iodomethane, Chem. Phys. Lett. 399 (2004) 196–199.
[8] K.T. Mueller, G.C. Chingas, A. Pines, NMR probe for dynamic-angle spinning, Rev. Sci. Instrum. 62 (1991) 1445–1452.
[9] F.D. Doty, G. Entzminger, Y.A. Yang, Magnetism in high-resolution NMR probe design. II: HR MAS, Concepts Magn. Reson. 10 (1998) 239–260.

[10] M. Tomaselli, B.H. Meier, M. Baldus, J. Eisenegger, R.R. Ernst, An rf-driven nuclear spin-diffusion experiment using zero-angle sample spinning, Chem. Phys. Lett. 225 (1994) 131–139.
[11] F.D. Doty, High power flexible leads for DAS NMR, US Patents 6,198,284 (2001).
[12] E.K. Paulson, R.W. Martin, K.W. Zilm, Cross polarization, radio frequency field homogeneity, and circuit balancing in high field solid state NMR probes, J. Magn. Reson. 171 (2004) 314–323.
[13] R.W. Martin, E.K. Paulson, K.W. Zilm, Design of a triple resonance magic angle sample spinning probe for high field solid state nuclear magnetic resonace, Rev. Sci. Instrum. 74 (2003) 3045–3061.
[14] D.W. Alderman, D.M. Grant, Efficient decoupler coil design which reduces heating in conductive samples in superconducting spectrometers, J. Magn. Reson. 36 (1979) 447–451.
[15] E.K. Paulson, R.W. Martin, K.W. Zilm, Cross polarization, radio frequency field homogeneity, and circuit balancing in high field solid state NMR probes, J. Magn. Reson. 171 (2004) 314–323.
[16] F.D. Doty, G. Entzminger, Y.A. Yang, Magnetism in high-resolution NMR probe design. I: general methods, Concepts Magn. Reson. 10 (1998) 133–156.
[17] B.M. Fung, A.K. Khitrin, K. Ermolaev, An improved broadband decoupling sequence for liquid crystals and solids, J. Magn. Reson. 142 (2000) 97–101.